Multimillimetre-large superlattices of air-stable iron–cobalt nanoparticles

CÉLINE DESVAUX[1,2], CATHERINE AMIENS[1], PETER FEJES[3], PHILIPPE RENAUD[2], MARC RESPAUD[4], PIERRE LECANTE[5], ETIENNE SNOECK[5] AND BRUNO CHAUDRET[1]*

[1]Laboratoire de Chimie de Coordination du CNRS, 205, route de Narbonne, 31077 Toulouse Cedex 04, France
[2]Freescale Semiconductor, le Mirail BP 1029, 31023 Toulouse Cedex, France
[3]Freescale Semiconductor, Inc., 2100 E. Elliot Road, Tempe, Arizona-85824, USA
[4]Laboratoire de la Physique de la Matière Condensée, INSA, 135 avenue de Rangueil, 31077 Toulouse, France
[5]Centre d'Elaboration des Matériaux et d'Etude Structurale, 29, rue Jeanne Marvig, BP94347, 31055 Toulouse Cedex 04, France
*e-mail: chaudret@lcc-toulouse.fr

Published online: 11 September 2005; doi:10.1038/nmat1480

Self-organization of nanoparticles into two- and three-dimensional superlattices on a large scale is required for their implementation into nano- or microelectronic devices[1,2]. This is achieved, generally after a size-selection process[3,4], through spontaneous self-organization on a surface[5–11], layer-by-layer deposition[12] or the three-layer technique of oversaturation[3,14], but these techniques consider superlattices of limited size. An alternative method developed in our group involves the direct formation in solution of crystalline superlattices, for example of tin nanospheres, iron nanocubes or cobalt nanorods, but these are also of limited size[15–17]. Here, we report the first direct preparation in solution of multimillimetre-sized three-dimensional compact superlattices of nanoparticles. The 15-nm monodisperse FeCo particles adopt an unusual short-range atomic order that transforms into body-centred-cubic on annealing at 500 °C. The latter process produces an air-stable material with magnetic properties suitable for radiofrequency applications.

The fabrication of small, low-consumption and high-performance inductors that are needed for the development of portable communication requires the deposition of a soft ferromagnetic layer with a high permeability value and a ferromagnetic resonance beyond the operating frequency. High permeability, in turn, requires homogeneous nanomaterials, with a narrow distribution of local magnetic field in order to get a sharper resonance. This could be achieved in organized nanostructured materials consisting of monodisperse soft ferromagnetic nanoparticles. Techniques generally use radiofrequency magnetron sputter deposition[18–20] or electroplating[21]. An alternative approach could use self-assembled Fe–Co nanoparticles, but would, in turn, raise several problems, namely: (i) organization of the particles into very large two- or three-dimensional superlattices (several millimetres or larger), (ii) control of the interparticle distance and of the overall geometry of the nanomaterial in order to obtain reproducible component performances, (iii) stability in air and (iv) manufacturability of the material. The FeCo nanoparticles or nanowires reported so far are dispersed in films or gels and therefore not suitable for radiofrequency applications, essentially because of the low metal volume fraction[22–24].

Bimetallic nanoparticles (CoRu, CoRh, CoPt or RuPt) have been obtained in our group by co-decomposition under H_2 of appropriate organometallic precursors[25]. A similar route leads to FeCo nanoparticles using $Fe(CO)_5$ (**1**), $Co(\eta^3\text{-}C_8H_{13})(\eta^4\text{-}C_8H_{12})$ (**2**) and $Co(N(SiMe_3)_2)_2$ (**3**) (ref. 26) as precursors. The stoichiometry 1 equiv. Co:2 equiv. Fe was chosen to lead to the correct composition of the final product. In a typical reaction, the precursors are reacted with H_2 at a pressure of 3 bars in toluene at 150 °C for 48 h in the presence of a mixture of 1 equiv. hexadecylamine and 1 equiv. oleic acid. A solid, consisting of millimetre-long black needles or plates, precipitates in high yield (typically 97% based on cobalt) from the solution. The needles are collected on a stirring bar, whereas the plates form when no stirring bar is present during the synthetic process (Fig. 1a).

Using either **1** and **2** or **1** and **3** as precursors, the resulting nanomaterials (**NM1** and **NM2**, respectively) were found by elemental analysis to show the target stoichiometry, namely $Fe_{0.61}Co_{0.39}$ and $Fe_{0.58}Co_{0.42}$, associated with a metal weight fraction of 75 and 80%, respectively. Transmission electron microscopy (TEM) measurements carried out directly on both **NM1** and **NM2** proved difficult and only showed the particles on the edges of the needles. However, after redissolution in the presence of excess ligands, well-dispersed spherical particles of around 15 nm mean size and low dispersity of size were visible. High-resolution electron microscopy (HREM) micrographs of **NM1** show a non-periodic contrast that differs from that expected in an amorphous material (Fig. 2). The Fourier transform of such HREM images reveals an intense diffraction ring at 0.2 nm^{-1} attributed to periodicity limited to domains of around 2 nm within the particle. Under the electron beam, the structure of the particles changes towards the body-centred-cubic periodic structure of bulk

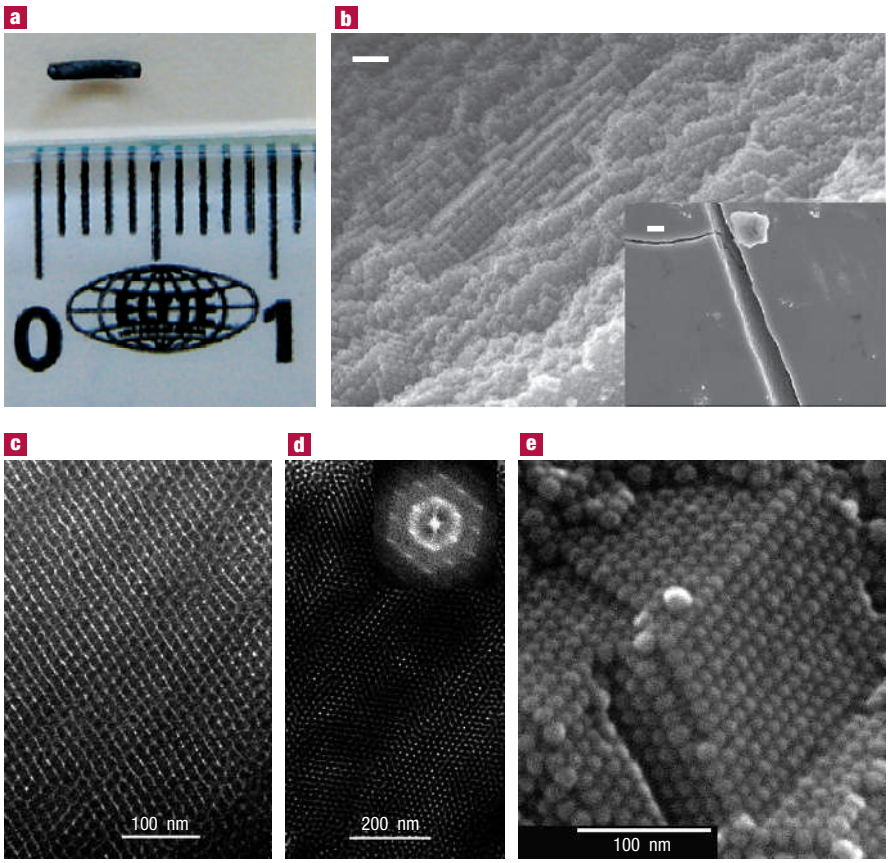

Figure 1 Global views of Fe–Co supercrystals from a macroscopic to a nanometric scale. a, Photograph of one 4-mm-long **NM1** supercrystal. **b**, SEM–FEG micrographs of a **NM1** supercrystal; scale bar = 10 nm, inset scale bar = 1 μm. **c**,**d**, TEM micrographs after ultramicrotomy of **NM1** nanoparticles (inset in **d**: Fourier transform of the image). **e**, SEM–FEG micrograph of a broken **NM1b** supercrystal.

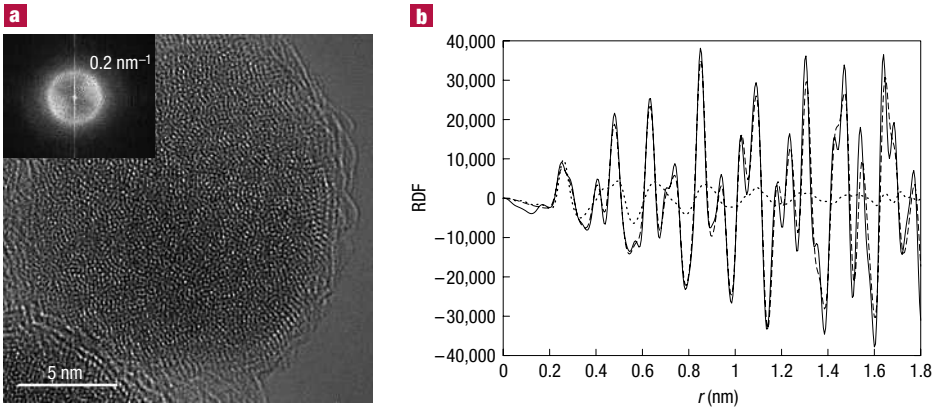

Figure 2 Structural analysis of Fe–Co nanoparticles. a, HREM micrograph and Fourier transform (inset) of one **NM1** nanoparticle. **b**, Radial distribution function (RDF) obtained by WAXS of **NM1** (dotted line), **NM1an** (dashed line) and a model (FeCo body-centred-cubic; full line); *r* is the interatomic distance.

FeCo, suggesting that this non-periodic structure of the particles is metastable. The diffraction pattern only shows a few broad peaks that do not match any common phase for iron, cobalt or an alloy. Furthermore, the HREM studies show the absence of significant oxidation of these particles (Fig. 2), although we cannot exclude the presence of a few atomic layers of surface oxidation. Wide-angle X-ray scattering (WAXS) experiments were also carried out on the material. After Fourier transform, the radial distribution function (Fig. 2b) shows a mean bond length of 0.260 nm consistent with a Fe–Co alloy. The coherence length of the particles is close to 2 nm, in agreement with HREM results, but much shorter than the real size of the particles. All of these

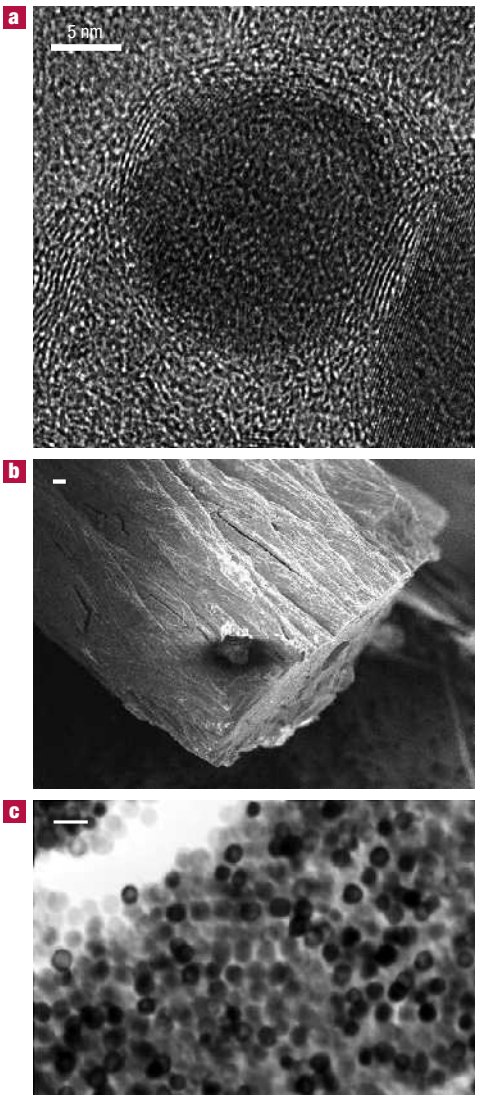

Figure 3 Scattering and TEM analysis of annealed Fe–Co nanoparticles. **a**, HREM micrograph of particle of **NMan**; scale bar = 5 nm. **b**, SEM–FEG micrograph of one **NMan** supercrystal; scale bar = 10 μm. **c**, TEM micrograph of **NMan** after ultramicrotomy; scale bar = 20 nm.

elements clearly indicate that the particles lack long-range atomic order and adopt a structure close to those observed for small Co and Fe nanoparticles in ref. 27, and to the ε cobalt phase discovered in ref. 28. Parametric endo/exoatmospheric lethality simulation (PEELS) analysis carried out on isolated particles suggests a surprising onion-like structure consisting of a cobalt core surrounded by an iron shell, itself surrounded by a cobalt layer (Supplementary Information, Fig. S3). As the PEELS samples had to be handled in air for a short time, the presence of some surface ferrite layer is not excluded. Scanning electron microscopy with field emission gun (SEM–FEG) analysis of several millimetre-sized solids showed a very densely packed arrangement of the particles that tends to crack owing to the high vacuum in the microscope chamber. The induced sharp ridges reveal the inner organization of the solids showing close-packed self-organized particles within millimetre-sized superstructures (Fig. 1b). TEM experiments performed on thin samples prepared by ultramicrotomy confirm the hexagonal two-dimensional packing of 15-nm-diameter monodisperse nanoparticles (Fig. 1c,d). The inset to Fig. 1d is a Fourier transform performed on the whole TEM image. The discrete reflections and the sixfold symmetry of the Fourier transform indicate that this regular organization remains over regions at least as large as 1 μm even if stacking faults can be observed in several regions. Owing to the large parameter of the supercrystal (~15 nm), its symmetry is difficult to explain by electron diffraction techniques. Interestingly, an optimization of the synthesis was carried out using one extra equivalent of stearic acid (**NM1b**) leading to very large supercrystals of otherwise similar particles. In this case, the organization is also visible throughout the supercrystals and local face-centred-cubic packing is revealed by SEM on a broken supercrystal (Fig. 1e). Spontaneous formation of nanocrystal superlattices has been observed in the case of tin[15] on precipitation of nanoparticles in the presence of an amine and an ammonium salt, but not for millimetre-sized crystals. In the field of magnetic materials, $CoPt_3$ superlattices with sizes up to 20 μm have been achieved, but the use of the three-layer technique of oversaturation was needed to generate the superlattices after the formation of the particles[14]. We benefit both from the potential presence of charges due to proton transfer between acid and amine and from the dipolar couplings between the particles aggregating them in solution. Both effects will induce a precipitation of the particles shown to favour formation of regular superlattices in the case of tin[15]. The regularity of the precipitated structure is due to the monodispersity of the particles. This, in turn, may result from the synthesis method, which uses organometallics and dihydrogen that both favour redistribution of atoms between nanoparticles and size homogeneity[17]. For **NM2**, SEM–FEG observations showed the presence of large superstructures of spherical particles of 15 nm mean diameter with a very low size distribution. Despite the apparent densely packed assembly of the particles, no clear long-range organization was detected either by SEM or by TEM after ultramicrotomy.

Squid measurements show a ferromagnetic behaviour at room temperature for **NM1** with a saturation magnetization (M_s) of 160 A m^2 kg$^{-1}_{FeCo}$, corresponding to a magnetic moment per metal atom of $\mu = 1.71\ \mu_B$ (where μ_B is the Bohr magnetron) and a coercive field $\mu_0 H_c$ of 0.01 T at 2 K and 0.3 mT at 300 K. Corresponding values for **NM2** were a M_s of 183 A m^2 kg$^{-1}_{FeCo}$, a magnetic moment per metal atom of $\mu = 1.95\ \mu_B$ and a $\mu_0 H_c$ of 0.01 T at 2 K and 1.1 mT at 300 K. The difference in M_s between **NM1** and **NM2** could be related to the different precursors. An excess amine is produced in the case of **NM2**, which has been shown to be innocuous for the magnetic properties of nanoparticles in contrast to CO or oxo groups.

Both **NM1** and **NM2** were found to slowly oxidize in the presence of air leading to the formation of a crystalline oxide shell (Supplementary Information, Fig. S1), probably a ferrite as shown in ref. 29, and to a decrease of the magnetic properties of the material (after 48 h $M_s = 130$ A m^2 kg$^{-1}_{FeCo}$, $\mu = 1.33\ \mu_B$, $\mu_0 H_c = 0.0064$ T at 300 K) concomitant with a slight shift in the hysteresis loop as expected. In order to circumvent this problem the particles were annealed under argon at 500 °C for 30 min. This thermal treatment produced new materials (**NM1an** and **NM2an**), but did not change either the size or shape of the individual particles or the shape of the superstructures. The organization of the nanoparticles inside the superstructures may, however, have been altered as no large organized arrays could be clearly shown by SEM or TEM after ultramicrotomy (Fig. 3). This probably results from the shrinking of the organic shell of the particles owing to the graphitization process and therefore from the possible mobility of the particles inside the superlattice. After annealing, the particles adopt the body-centred-cubic structure of bulk FeCo

as determined by both WAXS and HREM, hence confirming the metastable nature of the original atomic organization inside each particle. In addition, the coherence length derived from WAXS spectra shows a net increase, in agreement with a much better crystallinity inside the particles. Furthermore, the annealing process also leads to the formation of a carbon shell of around 2 nm width at the surface of the particles as shown by HREM (Fig. 3)[30]. This layer was found to protect the particles efficiently from oxidation (no noticeable change in the magnetic properties after two weeks of exposure to air). Finally, the annealing process leads to materials of higher weight fraction (90% for **NM1an** and 87% for **NM2an**). In these materials, the iron and cobalt atomic distribution within individual nanoparticles is homogeneous, as determined by PEELS, and the magnetic properties are strongly improved, as a result of the phase transition, as magnetization values are close to those expected for the bulk alloy ($M_s = 220$ A m^2 kg$^{-1}_{FeCo}$, $\mu = 2.25\ \mu_B$, $\mu_0 H_c = 0.015$ T at 300 K, 0.018 T at 2 K; $M_s = 245$ A m^2 kg$^{-1}_{FeCo}$ for bulk FeCo) both for **NM1an** and **NM2an** (Supplementary Information, Fig. S2). As suggested in ref. 30, the increase of the magnetic moment after annealing could be attributed to the disordered–ordered phase transition, the relative low magnetization observed before annealing being a consequence of the disordered structure. It is worth noting that this structural transition does not affect the magnetization process, because all of the nanomaterials described in this paper have small coercive fields and remanence magnetizations. Considering the magnetocrystalline anisotropy, the blocking temperature of isolated nanoparticles should be in the range of 50–70 K. In all cases, the large magnetic volume fraction, in the range of 40–50%, induces large dipolar fields that are stronger than the anisotropy field, which gives the main contribution to the energy barrier. This implies that the supercrystals adopt an antiferromagnetic structure arising from the dominant dipolar interactions[31]. This kind of nanostructured material fulfils the requirements for a high permeability in the gigahertz range. The measurements of the permeability properties are in progress. Preliminary experiments show a ferromagnetic resonance beyond 4 GHz. This study therefore demonstrates that the organometallic approach is adapted to the synthesis of nanomaterials of controlled size, organization and physical properties, which are then able to be implemented in low-consumption microelectronic devices.

METHODS

All non-commercial compounds were prepared under argon by using standard Schlenck techniques. A glove box was used for the preparation of the starting solutions. Toluene was purchased from SDS, distilled over sodium and degassed through three freeze–pump–thaw cycles. Hexadecylamine and $Fe(CO)_5$ were purchased from Fluka and Aldrich, respectively. The elemental analyses were performed by the Service Central d'Analyse, Département Analyse Elementaire in Vernaison, CNRS, France. The TEM studies were carried out on a JEM 200CX, 200 kV, resolution 4, 5 Å, the HRTEM studies on a JEOL-2010, 200 kV, resolution 2.3 Å, the SEM–FEG studies on a JEOL JSM 6700F, 0.5 to 30 kV and the PEELS studies on a Philips CM200 FEG-TEM apparatus. The Squid magnetometer was a MPMS 5 Quantum Design. WAXS measurements were performed at CEMES on a dedicated two-axis diffractometer at molybdenum wavelength (0.071069 nm). Measurement time was typically 20 h per sample. Pure sample powders were sealed inside thin-walled glass cpillaries 1.5 mm in diameter. Intensity was reduced by subtraction of components independent of the structure, and then Fourier transformed.

$CO(\eta^3\text{-}C_8H_{13})(\eta^4\text{-}C_8H_{12})$ AND $CO(N(SIME_3)_2)_2$

The synthetic procedures are described in the literature[32,33].

TYPICAL PROCEDURES LEADING TO **NM1**, **NM1B** AND **NM2**

In the glove box, 1 mmol of hexadecylamine (241 mg), 1 mmol of oleic acid (282 mg) and 1 mmol of cobalt precursor (for example, 276 mg of $Co(\eta^3\text{-}C_8H_{13})(\eta^4\text{-}C_8H_{12})$ or 379 mg of $Co(N(SiMe_3)_2)_2$) are introduced into a Fisher Porter bottle. 50 ml of degassed and distilled toluene are added followed by 2 mmol of iron precursor $Fe(CO)_5$ (0.27 ml). The bottle is then conditioned under H_2 at a pressure of 3 bars and placed in an oil bath at 150 °C for 48 h. At the end of the reaction, H_2 is evacuated and the supernatant removed. If magnetic agitation is used during the synthesis, the black material obtained is found on the stirring bar; if no agitation is used during the synthesis, the black powder lies at the bottom of the Fisher Porter bottle. In both cases, the product is dried under vacuum for 12 h and a powder is collected in the glove box (mass $m = 150$ mg). Considering the weight fraction of metal of the samples (75% for **NM1** and 80% for **NM2**) and their relative composition ($Fe_{0.61}Co_{0.39}$ for **NM1** and $Fe_{0.58}Co_{0.42}$ for **NM2**), the yield related to each metal can be calculated as $\eta_{Fe} = 73\%$ and $\eta_{Co} = 97\%$.

A procedure totally similar to that used for **NM1** but adding initially 1 extra equiv. stearic acid to the other reagents leads to a more regular structure, **NM1b** (yield $\eta_{Co} = 97\%$).

TYPICAL PROCEDURES LEADING TO **NMAN1** AND **NMAN2**

150 mg of **NM1** or **NM2** are transferred in the glove box into a quartz tube that is then placed in an oven to be annealed. The temperature ramp is as follows: (i) from room temperature to 300 °C, 10 °C min^{-1}; (ii) from 300 to 500 °C, 5 °C min^{-1}; (iii) 30 min at 500 °C then natural cooling back to room temperature. 120 mg of annealed material that has a metallic aspect is then collected in the glove box.

Received 17 March 2005; accepted 28 July 2005; published 11 September 2005.

References

1. Alivisatos, A. P. Semiconductor clusters, nanocrystals and quantum dots. *Science* **271,** 933–937 (1996).
2. Carter, J. D., Cheng, G. & Guo, T. Growth of self-aligned crystalline cobalt silicide nanostructures from Co nanoparticles. *J. Phys. Chem. B.* **108,** 6901–6904 (2004).
3. Wang, Z. L. *et al.* Superlattices of self-assembled tetrahedral Ag nanocrystals. *Adv. Mater.* **10,** 808–812 (1998).
4. Park, J. *et al.* Ultra-large-scale syntheses of monodisperse nanocrystals. *Nature Mater.* **3,** 891–895 (2004).
5. Legrand, J., Ngo, A. T., Petit, C. & Pileni, M. P. Domain shapes and superlattices made of cobalt nanocrystals. *Adv. Mater.* **13,** 58–62 (2001).
6. Sigman, M. B., Saunders, A. E. & Korgel, B. A. Metal nanocrystal superlattice nucleation and growth. *Langmuir* **20,** 978–983 (2004).
7. Hoogenboom, J. P. *et al.* Template induced growth of close-packed colloidal crystals during solvent evaporation. *Nano Lett.* **4,** 205–208 (2004).
8. Sun, S. & Murray, C. B. Synthesis of monodisperse cobalt nanocrystals and their assembly into magnetic superlattices. *J. Appl. Phys.* **85,** 4325–4330 (1999).
9. Stoeva, S. I. *et al.* Face-centered cubic and hexagonal closed-packed nanocrystal superlattices of gold nanoparticles prepared by different methods. *J. Phys. Chem. B* **107,** 7441–7448 (2003).
10. Sun, S., Murray, C. B., Weller, D., Folks, L. & Moser, A. Monodisperse FePt nanoparticles and ferromagnetic FePt nanocrystal superlattices. *Science* **287,** 1989–1992 (2000).
11. Lisiecki, I., Albouy, P. A. & Pileni, M. P. Face-centered cubic "supracrystals" of cobalt nanocrystals. *Adv. Mater.* **15,** 712–716 (2003).
12. Wang, Z. L. Nanobelts, nanowires, and nanodiskettes of semiconducting oxides—from materials to nanodevices. *Adv. Mater.* **15,** 432–436 (2003).
13. Talapin, D. V. *et al.* A new approach to crystallization of CdSe nanoparticles into ordered three-dimensional superlattices. *Adv. Mater.* **13,** 1868–1871 (2001).
14. Shevchenko, E. V. *et al.* Colloidal synthesis and self-assembly of $CoPt_3$ nanocrystals. *J. Am. Chem. Soc.* **124,** 11480–11485 (2002).
15. Soulantica, K., Maisonnat, A., Fromen, M. C., Casanove, M. J. & Chaudret, B. Spontaneous formation of ordered 3D super-lattices of nanocrystals from polydisperse colloidal solutions. *Angew. Chem. Int. Edn Engl.* **42,** 1945–1949 (2003).
16. Dumestre, F., Chaudret, B., Amiens, C., Renaud, P. & Fejes, P. Superlattices of iron nanocubes synthesized from $Fe[N(SiMe_3)_2]_2$. *Science* **303,** 821–823 (2004).
17. Dumestre, F. *et al.* Unprecedented crystalline super-lattices of monodisperse cobalt nanorods. *Angew. Chem. Int. Edn Engl.* **42,** 5213–5216 (2003).
18. Duc, N. H., Danh, T. M., Tuan, N. A. & Teillet, J. Large magnetostrictive susceptibility in Tb-FeCo/FeCo multilayers. *Appl. Phys. Lett.* **78,** 3648–3650 (2001).
19. Cooke, M. D. *et al.* The effect of thermal treatment, composition and substrate on the texture and magnetic properties of FeCo thin films. *J. Phys. D* **33,** 1450–1459 (2000).
20. Albert, F. J., Katine, J. A., Buhrman, R. A. & Ralph, D. C. Spin-polarized current switching of a Co thin film nanomagnet. *Appl. Phys. Lett.* **77,** 3809–3811 (2000).
21. Garcia-Miquel, H., Bhagat, S. M., Lofland, S. E., Kurlyandskaya, G. V. & Svalov, A. V. Ferromagnetic resonance in FeCoNi electroplated wires. *J. Appl. Phys.* **94,** 1868–1872 (2003).
22. Willard, M. A., Laughlin, D. E. & McHenry, M. E. Ferromagnetic resonnance and eddy currents in high-permeable thin films. *J. Appl. Phys.* **87,** 7091–7096 (2000).
23. Corrias, A., Casula, M. F., Falqui, A. & Paschina, G. Evolution of the structure and magnetic properties of FeCo nanoparticles in an alumina aerogel matrix. *Chem. Mater.* **16,** 3130–3138 (2004).
24. Tang, S. L. *et al.* Nanostructure and magnetic properties of $Fe_{69}Co_{31}$ nanowire arrays. *Chem. Phys. Lett.* **384,** 1–4 (2004).
25. Zitoun, D. *et al.* Synthesis and magnetism of Co_xRh_{1-x} and Co_xRu_{1-x} nanoparticles. *J. Phys. Chem. B* **107,** 6997–7005 (2003).
26. Margeat, O., Amiens, C., Chaudret, B., Lecante, P. & Benfield, R. E. Chemical control of structural and magnetic properties of cobalt nanoparticles. *Chem. Mater.* **17,** 107–111 (2005).
27. Dassenoy, F. *et al.* Experimental evidence of structural evolution in ultrafine cobalt particles stabilized in different polymers. From a polytetrahedral arrangement to hexagonal structure. *J. Chem. Phys.* **112,** 8137–8145 (2000).
28. Dinega, D. P. & Bawendi, M. G. A solution-phase chemical approach to a new crystal structure of cobalt. *Angew. Chem. Int. Edn* **38,** 1788–1791 (1999).
29. Turgut, Z., Nuhfer, N. T., Piehler, H. R. & McHenry, M. E. Magnetic properties and microstructural observations of oxide coated FeCo nanocrystals before and after compaction. *J. Appl. Phys.* **85,** 4406–4408 (1999).
30. Turgut, Z., Huang, M.-Q., Gallagher, K., McHenry, M. E. & Majetich, S. A. Magnetic evidence for structural phase transformation in FeCo nanpocrystals produced by a carbon arc. *J. Appl. Phys.* **81,** 4039–4041 (1997).
31. Kechrakos, D. & Trohidou, K. N. Magnetic properties of dipolar interacting single domain particles. *Phys. Rev. B* **58,** 12169–12177 (1998).
32. Otsuka, S. & Rossi, M. Synthesis, structure, and properties of -cyclo-octenyl–cyclo-octa-1,5-dienecobalt. *J. Chem. Soc. A* 2630–2633 (1968).
33. Andersen, R. A. *et al.* Synthesis of bis[bis(trimethylsilyl)amido]iron(II). Structure and bonding in $M[N(SiMe_3)_2]_2$ (M = Mn, Fe, Co): Two coordinate transition-metal amides. *Inorg. Chem.* **27,** 1782–1786 (1988).

Acknowledgements

The authors thank CNRS and FREESCALE S. P. S. for support, M. Vincent Collière, Lucien Datas and TEMSCAN service (Université Paul Sabatier Toulouse) for TEM, Mlle Isabelle Fourquaux and Mr Bruno Payré (CMEAB, Université Paul Sabatier Toulouse) for ultramicrotomy and Alain Mari for the magnetic measurements.
Correspondence and requests for materials should be addressed to B.C.
Supplementary Information accompanies this paper on www.nature.com/naturematerials.

Competing financial interests

The authors declare that they have no competing financial interests.